Controlled Synthesis and Optical Properties of Colloidal Ternary Chalcogenide $CuInS_2$ Nanocrystals

Haizheng Zhong,[†,‡] Yi Zhou,[†,‡] Mingfu Ye,[†,‡] Youjun He,[†,‡] Jianping Ye,[§] Chang He,[†] Chunhe Yang,[†] and Yongfang Li*[,†]

Beijing National Laboratory for Molecular Sciences, Chinese Academy of Sciences Key Laboratory of Organic Solids, Institute of Chemistry, Chinese Academy of Sciences, Beijing 100190, China, Graduate University of the Chinese Academy of Sciences, Beijing 100039, China, and Chinese Academy of Sciences Key Laboratory of Photochemistry, Institute of Chemistry, Chinese Academy of Sciences, Beijing 100080, China

Received March 8, 2008. Revised Manuscript Received July 25, 2008

A facile method for the synthesis of size- and shape-controlled $CuInS_2$ semiconductor nanocrystals was developed by thermolysis of a mixed solution of CuAc, $In(Ac)_3$ (molar ratio of CuAc to $In(Ac)_3$ = 1:1) and dodecanethiol in noncoordinating solvent 1-octadecene (ODE) at 240 °C. $CuInS_2$ nanoparticles with size of 2 to ~5 nm and nanorods with aspect ratio of 1 to ~3 were obtained by adjusting the reaction parameters such as temperature and time. The as-prepared nanoparticles were characterized by X-ray diffraction (XRD), X-ray photoelectron spectroscopy (XPS), transmission electron microscopy, selected area electron diffraction spectroscopy, inductively coupled plasma atomic emission spectroscopy, UV−vis absorption, and photoluminescence (PL) spectroscopy. The nanoparticle solutions exhibit tunable absorption and PL spectra with the absorption edge ranging from 550 to 750 nm and PL emission peaks from 600 to 750 nm, indicating a strong size-dependent quantum confinement effect. Optical measurements of the $CuInS_2$ nanoparticles demonstrated that their optical properties are related to donor−acceptor defects, size-dependent quantum confined effects, and surface defects. The PL decay curve of $CuInS_2$ nanoparticles has a triple exponential characteristic with lifetimes of 4−12, 28−60, and 140−300 ns, respectively, and the PL emission with the longest lifetime (140−300 ns) occupied 40−80% of the PL emission of the samples. These results imply that the room-temperature PL emission of $CuInS_2$ nanoparticles involves three types of recombination: band exciton recombination, surface-related recombination, and donor−acceptor defects recombination. Among them, the PL emission from donor−acceptor defects occupied a large amount.

Introduction

Colloidal semiconductor nanocrystals have attracted great attention in recent years, for their novel properties and promising technological applications in various fields.[1] Semiconductor nanocrystals have many fascinating properties such as tunable absorption and emission,[1a] high-efficiency interface charge separation,[2a] spatial separation,[2b] multiexcitons generation,[2c,d] and easy chemical modification and processing,[2e] which make semiconductor nanocrystals suitable for next-generation photovoltaic applications.[3] By introducing semiconductor nanocrystals into conjugated polymer matrix or spin-coating two layers of semiconductor nanocrystals with type II band offset, obvious photoinduced charge-transfer effects were observed, and the power conversion efficiency of the devices has approached 3%.[1d,4]

The composition, size, shape, and structure of the nanocrystals play a very important role in the performance of the nanocrystal-based solar cells.[1d,4,5] Up to now, a series of colloidal semiconductor nanocrystals such as CdSe, CdTe, CdS, PbSe, etc. have been controllably prepared and investigated for application in the nanocrystal-based solar cells.[5] However, most of the semiconductor nanocrystals

* Corresponding author. E-mail: liyf@iccas.ac.cn.
† Chinese Academy of Sciences Key Laboratory of Organic Solids.
‡ Graduate University of the Chinese Academy of Sciences.
§ Chinese Academy of Sciences Key Laboratory of Photochemistry.

(1) (a) Alivisatos, A. P. *Science* **1996**, *271*, 933–937. (b) Murray, C. B.; Kagan, C. R.; Bawendi, M. G. *Annu. Rev. Mater. Sci.* **2000**, *30*, 545–610. (c) Bruchez, M.; Moronne, M.; Gin, P.; Alivisatos, A. P. *Science* **1998**, *281*, 2013–2016. (d) Huynh, W. U.; Dittmer, J. J.; Alivisatos, A. P. *Science* **2002**, *295*, 2425–2427. (e) Sun, Q. J.; Wang, Y. A.; Li, L. S.; Wang, D. Y.; Zhu, T.; Xu, J.; Yang, C. H.; Li, Y. F. *Nat. Photonics* **2007**, *1*, 717–722.

(2) (a) Robel, I.; Kuno, M.; Kamat, P. V. *J. Am. Chem. Soc.* **2007**, *128*, 4136–4137. (b) Kumar, S.; Jones, M.; Lo, S. S.; Scholes, G. D. *Small* **2007**, *3*, 1633–1639. (c) Klimov, V. I. *Annu. Rev. Phys. Chem.* **2007**, *58*, 635–673. (d) Nozik, A. J. *Inorg. Chem.* **2005**, *44*, 6893–6899. (e) Konstantatos, G.; Howard, I.; Fischer, A.; Hoogland, S.; Clifford, J.; Klem, E.; Levina, L.; Sargent, E. H. *Nature* **2006**, *442*, 180–183.

(3) (a) Nozik, A. J. *Physica E* **2002**, *14*, 115–120. (b) Raffaelle, R. P.; Castro, S. L.; Hepp, A. F.; Bailey, S. G. *Prog. Photovoltaics* **2002**, *10*, 433–439. (c) Kamat, P. V. *J. Phys. Chem. C* **2007**, *111*, 2834–2860. (d) Kumar, S.; Scholes, G. D. *Microchim. Acta* **2008**, *160*, 315–325.

(4) (a) Gur, I.; Fromer, N. A.; Geier, M. L.; Alivisatos, A. P. *Science* **2005**, *310*, 462–465. (b) Sun, B. Q.; Snaith, H. J.; Dhoot, A. S.; Westenhoff, S.; Greeham, N. C. *J. Appl. Phys.* **2005**, *97*, 014914. (c) Gur, I.; Fromer, N. A.; Chen, C. P.; Kanaras, A. G.; Alivisatos, A. P. *Nano Lett.* **2007**, *7*, 409–414.

(5) (a) Sun, B. Q.; Marx, E.; Greenham, N. C. *Nano Lett.* **2003**, *3*, 961–964. (b) Kumar, S.; Nann, T. *J. Mater. Res.* **2004**, *19*, 1990–1994. (c) Zhong, H. Z.; Zhou, Y.; Yang, Y.; Yang, C. H.; Li, Y. F. *J. Phys. Chem. C* **2007**, *111*, 6538–6543. (d) Zhou, Y.; Li, Y. C.; Zhong, H. Z.; Hou, J. H.; Ding, Y. Q.; Yang, C. H.; Li, Y. F. *Nanotechnology* **2006**, *17*, 4041–4047. (e) McDonald, S. A.; Konstantatos, G.; Zhang, S. G.; Cyr, P. W.; Klem, E. J. D.; Levina, L.; Sargent, E. H. *Nat. Mater.* **2005**, *4*, 138–142. (f) Cui, D. H.; Zhu, T.; Paradee, G.; Ashok, S.; Gerhold, M. *Appl. Phys. Lett.* **2006**, *88*, 138111.

10.1021/cm8006827 CCC: $40.75
Published on Web 09/24/2008

contain toxic heavy metals such as Cd, Pb, Te, and so on, which limited their applications. For this reason, people turned their attentions to ternary I−III−VI compounds such as $CuInS_2$ and $CuInSe_2$ which have shown attractive device performance in thin film solar cells.[6]

$CuInS_2$ is of particular interest in photovoltaic applications for its high energy conversion efficiency, high absorption coefficient, and low toxicity. The solar energy conversion efficiency of thin film devices based on $CuInS_2$ has reached 13%.[7] Theoretical calculations indicate that the Wannier−Mott bulk exciton radius of $CuInS_2$ is 4.1 nm.[8] It was expected that the $CuInS_2$ nanocrystals with size comparable to Wannier−Mott bulk exciton radius are suitable materials for nanocrystal solar cells and nontoxic luminescent compounds. Thus, it is of great importance to synthesize the colloidal $CuInS_2$ nanoparticles with their size smaller than 10 nm.

Several approaches have been employed to prepare $CuInS_2$ nanocrystals including a solvothermal method,[9−11] a precursor decomposition method,[12−14] and hot injection techniques.[15−17] $CuInS_2$ nanoparticles with size smaller than 10 nm and room-temperature PL emission can be readily prepared by the precursor decomposition approach.[12−14] The precursor approaches are based on decomposing the precursor upon thermal heating or microwave or UV irradiation. For example, Castro et al. reported a thermal decomposition method of single-source precursor $[(PPh_3)_2CuIn(SEt)_4]$ to synthesize colloidal $CuInS_2$ nanoparticles.[12] Nairn et al. prepared 2 nm sized $CuInS_2$ nanocrystals by UV irradiation on single-molecular precursor $[(PPh_3)_2CuIn(SEt)_4]$.[13] Recently, Gardner et al. prepared the $CuInS_2$ semiconductor nanoparticles by microwave irradiation of the similar precursors.[14]

Here, we developed a facile method to synthesize $CuInS_2$ nanoparticles by thermolysis of a nontoxic mixture solution of copper(I) acetate, indium acetate, and alkylthiol mixture in a high boiling point solvent at 240 °C. The synthetic process does not use toxic compounds and does not need any presynthesis of the precursors. By scaling up of the reaction system, gram-scale or higher amounts of nanoparticles can be produced. The size, shape, and optical properties of the $CuInS_2$ nanocrystals can be easily controlled via adjusting the reaction temperature and reaction time. The optical properties of the as-prepared $CuInS_2$ nanocrystals were also investigated and discussed.

Experimental Section

Materials. Copper(I) acetate (CuAc, Strem Chemicals, 99%), indium(III) acetate ($In(Ac)_3$, Alfa Aesar, 99.999%), *n*-dodecanethiol (Alfa Aesar, 98%), 1-octadecene (ODE, Aldrich, 90%), methanol, acetone, chloroform, and toluene (Beijing Chemical Reagent Ltd. Co., China) are analytical reagents. Carbon-coated copper grids were obtained from Beijing Xin Xing Bai Rui Ltd. Co., China. All the chemicals were used as received without further purification.

Synthesis of $CuInS_2$ Nanocrystals. Typical synthesis of $CuInS_2$ nanoparticles was performed as follows: CuAc (24.4 mg, 0.2 mmol) and $In(Ac)_3$ (58.2 mg, 0.2 mmol) were mixed with 0.5 mL of dodecanethiol in a 25 mL three-necked bottle, and then 5 mL of ODE was added. The mixture system was degassed by argon flowing for 30 min. The system was subsequently heated to 240 °C and reacted for a fixed time; a deep red colloidal solution was obtained. During the course of the reaction, a small amount of sample was taken out via syringe at different times, and it was diluted to an optical density between 0.1−0.5 by the addition of chloroform to monitor the growth of $CuInS_2$ nanoparticles by recording UV−vis and PL spectra. Afterward, the reaction solution was cooled to 60 °C and precipitated by acetone. The flocculent precipitate was centrifuged, the upper layer liquid was decanted, and then the isolated solid was dispersed in toluene. The above centrifugation and isolation procedure was then repeated several times for purification of the prepared $CuInS_2$ nanocrystals. Finally, the $CuInS_2$ nanocrystals were redispersed into toluene or dried under vacuum for measurements.

Gram-scale synthesis of the $CuInS_2$ nanocrystals was conducted by the thermolysis of a mixture of 1.22 g of CuAc, 2.91 g of $In(Ac)_3$, 25 mL of dodecanethiol, and 250 mL of ODE in a 500 mL three-necked bottle at 240 °C for 2.5 h. The purification procedures are similar to the method mentioned above. After purification, the argon-flow-dried nanocrystals weighed about 2.0 g.

Characterization and Analysis. The sample for transmission electron microscopy (TEM) measurement was prepared by depositing one drop of a dilute toluene solution of the samples on a carbon-coated copper grid and drying at room temperature. Transmission electron microscopy and high-resolution transmission electron microscopy (HRTEM) observations were performed with a JEOL-2010 transmission electron microscope, accompanied by selected area electron diffraction (SAED). X-ray diffraction (XRD) patterns and small-angle XRD patterns were recorded by a Rigaku D/max-2400 diffractometer operated at 40 kV voltage and a 120 mA current with Cu Kα radiation; the powder samples were prepared by drying the purified product under vacuum. Fourier transform infrared (FTIR) spectra in the region of 700−4000 cm^{-1} were recorded on

(6) (a) Nanu, M.; Schoonman, J.; Goossens, A. *Nano Lett.* **2005**, *5*, 1716–1719. (b) Ng, M. T.; Boothroyd, C. B.; Vittal, J. J. *J. Am. Chem. Soc.* **2006**, *128*, 7118–7119. (c) Zhong, H. Z.; Li, Y. C.; Ye, M. F.; Zhu, Z. Z.; Zhou, Y.; Yang, C. H.; Li, Y. F. *Nanotechnology* **2007**, *18*, 025602. (d) Peng, H. L.; Schoen, D. T.; Meister, S.; Zhang, X. F.; Cui, Y. *J. Am. Chem. Soc.* **2007**, *129*, 34–35.
(7) Klaer, J.; Bruns, J.; Henninnger, R.; Siemer, K.; Klenk, R.; Ellmer, K.; Brauning, D. *Semicond. Sci. Technol.* **1998**, *13*, 1456–1458.
(8) The Bohr exciton radius is calculated by $r_B = (\varepsilon_{dot}/\mu)a_B$, $\mu = 1/(1/m_e^* + 1/m_h^*)$, where a_B is the hydrogen Bohr radius, ε_{dot} is the dielectric constant of the bulk material, and m_e^* and m_h^* are the reduced masses of the electron and hole. The values of $CuInS_2$ are 11 for ε_{dot}, 0.16 for m_e^*, and 1.3 for m_h^*, respectively.
(9) (a) Jiang, Y.; Wu, Y.; Mo, X.; Yu, W. C.; Xie, Y.; Qian, Y. T. *Inorg. Chem.* **2000**, *39*, 2964–2965. (b) Lu, Q. Y.; Hu, J. Q.; Tang, K. B.; Qian, Y. T.; Zhou, G. E.; Liu, X. M. *Inorg. Chem.* **2000**, *39*, 1606–1608. (c) Xiao, J. P.; Xie, Y.; Tang, R.; Qian, Y. T. *J. Solid State Chem.* **2001**, *161*, 179–183. (d) Cui, Y.; Ren, J.; Chen, G.; Qian, Y. T.; Xie, Y. *Chem. Lett.* **2001**, *3*, 236–237. (e) Ahn, S.; Kim, K. H.; Chun, Y. G.; Yoon, K. G. *Thin Solid Films* **2007**, *515*, 4036–4040.
(10) Du, W. M.; Qian, X. F.; Yin, J.; Gong, Q. *Chem. Eur. J.* **2007**, *13*, 8840–8846.
(11) (a) Das, K.; Dutta, D. P.; Chaudhuri, S. *Cryst. Growth Des.* **2007**, *7*, 1547–1552. (b) Dutta, D. P.; Sharma, G. *Mater. Lett.* **2006**, *60*, 2395–2398.
(12) (a) Castro, S. L.; Bailey, S. G.; Banger, K. K.; Hepp, A. F. *Chem. Mater.* **2003**, *15*, 3142–3147. (b) Castro, S. L.; Bailey, S. G.; Banger, K. K.; Hepp, A. F. *J. Phys. Chem. B* **2004**, *108*, 12429–12434.
(13) Nairn, J. J.; Schapiro, P. J.; Twamley, B.; Pounds, T.; Wandruszka, R. V.; Williams, M.; Wang, C. M.; Notton, M. G. *Nano Lett.* **2006**, *6*, 1218–1223.
(14) Gardner, J. S.; Shurdha, E.; Wang, C. M.; Lau, L. D.; Rodriguez, Park, J. J. *J. Nanopart. Res* **2008**, *10*, 633–641.
(15) Czekelius, C.; Hilgendorff, M.; Spanhel, L.; Bedja, I.; Lerch, M.; Muller, G.; Bloeck, U.; Su, D. S.; Giersig, M. *Adv. Mater.* **1999**, *11*, 643–646.
(16) Nakamura, H.; Kato, W.; Uehara, M.; Nose, K.; Omata, T.; Matsuo, S. O.; Miyazaki, M.; Maeda, H. *Chem. Mater.* **2006**, *18*, 3330–3335.
(17) Pan, D. C.; An, L. J.; Sun, Z. M.; Hou, W.; Yang, Y.; Yang, Z. Z.; Lu, Y. F. *J. Am. Chem. Soc.* **2008**, *130*, 5620–5621.

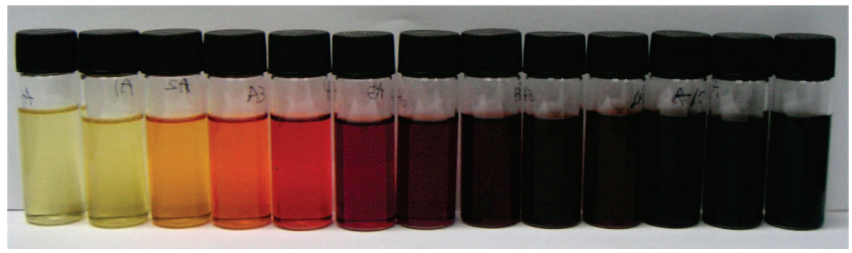

Figure 1. Photographs of the samples of 0.2 mmol of CuAc, 0.2 mmol of $In(Ac)_3$, and 0.5 mL of dodecanethiol in 5 mL of ODE after heating at 240 °C for (from left to right) 1, 3, 6, 10, 15, 20, 30, 60, 120, 180, 240, 300, and 360 min.

a Bruker Tensor 27. The ^1H NMR spectrum was measured on a Bruker DMX-400 spectrometer. The X-ray photoelectron spectroscopy (XPS) was collected on an ESCA Lab220I-XL X-ray photoelectron spectrometer using an Al Kα X-rays as the excitation source. The composition of the alloyed nanocrystals was measured by means of inductively coupled plasma atomic emission (ICP-AES) using a standard digestion method. The samples were prepared as follows: a fixed amount of $CuInS_2$ sample was mixed with 2 g of KOH and heated under 100 °C for 0.5 h; then the mixture was heated to 400 °C to make it melt into a liquid. After that, the mixture was cooled to room temperature. HCl solution (1%, wt %) was added into the mixture; then the mixture solution was transferred to a volumetric flask to get a 100 mL solution. UV−vis absorption spectra were recorded on a Jasco FP-6600 spectrophotometer. Steady-state photoluminescence (PL) spectra and photoluminescence excitation (PLE) were measured on a Jasco V-570 spectrophotometer. The PL quantum yield of the samples was determined using CdSe/CdS core/shell quantum dots (provided by Ocean Nanotech Ltd., U.S.A.) with known quantum yield as the standard, with a previously reported method.[18] PL dynamics were measured on Fluoromax-4 (Horiba Jobin Yvon) with excitation wavelength of 476 nm.

Results and Discussion

Synthesis and Characterization of $CuInS_2$ Nanoparticles. In recent years, many synthetic techniques of inorganic semiconductor nanocrystals such as hot injection, thermal decomposition of single precursor, seed catalytic growth, etc.[19] have been intensively investigated and achieved many exciting results in binary compound syntheses. However, only few of them can be adapted to synthesize ternary compound nanocrystals. In a ternary system, there are three elements involved in the reaction, and the reaction activity of the reagents related to the three elements should be considered. If the reaction activities of two metal precursors differ from each other, a separated nucleus will be generated and grow into heterostructures or even two compounds.[20] Recently, the single precursors containing the reactant compounds were successfully used to prepare ternary compounds. Molecular compounds such as $(Ph_3P)_2CuIn(SEt)_4$ and $(Ph_3P)_2CuIn(S^tBu)_4$ were first synthesized by Hirpo et al.[21] and subsequently used as precursors to prepare $CuInS_2$ thin films[22,23] and colloidal nanoparticles.[12−14] Structural characterization of the molecular precursor showed that the compound contains a planar "CuInSR" core.[21] So it can be induced that thiol groups may have a similar bonding ability to Cu and In and play a key role in forming $CuInS_2$ nanocrystals. A previous report has also proved that alkylthiol acted as the S source and ligand to control nanocrystal growth.[24]

Here we developed a simple copper(I) acetate, indium(III) acetate, and dodecanethiol system to synthesize $CuInS_2$ nanoparticles. Typical synthetic processes of the $CuInS_2$ nanoparticles were described in the Experimental Section. When heating a mixture of CuAc, $In(Ac)_3$, and dodecanethiol in the noncoordinating solvent ODE, it can be observed that the color of the mixed solution gradually turned from turbid yellow to clear yellow, to orange, to deep red, and finally dark, which indicates the formation of $CuInS_2$ nanoparticles (see Figure 1).

On the basis of the color change of the samples with reaction time, we expected that precursor compound may be formed first from the reaction of alkylthiol with two metal salts and then it decomposed into $CuInS_2$ nanoparticles. For confirming the expectation, an XRD measurement was taken to clarify the reaction process of the system. The XRD pattern of the sample prepared by heating 0.2 mmol of CuAc, 0.2 mmol of $InAc_3$, 0.5 mL of dodecanethiol in 5 mL of ODE at 210 °C for 10 min (see Figure 2a) indicates that a new intermediate compound, which may be ascribed to the $CuIn(SR)_x$ complex, was formed. The FTIR technique was used to investigate the formed intermediate compound. By comparing the FTIR spectra of the intermediate compound and that of the pure dodecanethiol (see Figure 2b), it was found that both have the sharp bands at 2923 and 2857 cm^{-1}, which can be assigned to the asymmetric methyl stretching and asymmetric and symmetric methylene stretching modes, respectively, whereas the intermediate compound did not

(18) Demas, J. N.; Crosby, G. A. *J. Phys. Chem.* **1971**, *75*, 991–1024.
(19) (a) Murry, C. B.; Norris, D. J.; Bawendi, M. C. *J. Am. Chem. Soc.* **1993**, *115*, 8706–8715. (b) Peng, L. H.; Peng, Z. A.; Peng, X. G. *Nano Lett.* **2001**, *1*, 333–337. (c) Peng, Z. A.; Peng, X. G. *J. Am. Chem. Soc.* **2001**, *123*, 183–184. (d) Li, Y. C.; Li, X. H.; Yang, C. H.; Li, Y. F. *J. Mater. Chem.* **2003**, *13*, 2641–2648. (e) Wang, F. D.; Dong, A. G.; Sun, J. W.; Tang, R.; Yu, H.; Buhro, W. E. *Inorg. Chem.* **2006**, *45*, 7511–7521.
(20) Choi, S. H.; Kim, E. G.; Hyeon, T. *J. Am. Chem. Soc.* **2006**, *128*, 2520–2521.
(21) Hirpo, W.; Dhingra, S.; Stuorik, A. C.; Kanatzidis, M. G. *J. Am. Chem. Soc.* **1993**, *115*, 3142–3147.
(22) (a) Banger, K. K.; Cowen, J.; Hepp, A. F. *Chem. Mater.* **2001**, *13*, 3827–3829. (b) Banger, K. K.; Jin, M. H. C.; Harris, J. D.; Fanwick, P. F.; Hepp, A. F. *Inorg. Chem.* **2003**, *24*, 7713–7715.
(23) (a) Banger, K. K.; Hollingsworth, J. A.; Harris, J. D.; Cowen, J.; Buhro, W. E.; Hepp, A. F. *Appl. Organomet. Chem.* **2002**, *16*, 617–627. (b) Hollingsworth, J. A.; Banger, K. K.; Jin, M. H. C.; Harris, J. D.; Cowen, J. E.; Bohannan, E. W.; Buhro, W.; Hepp, A. F. *Thin Solid Films* **2003**, *431*, 63–67.
(24) Chung, Y. S.; Jang, E. J.; Jun, S. N. *Nanotechnology* **2006**, *17*, 4806–4810.

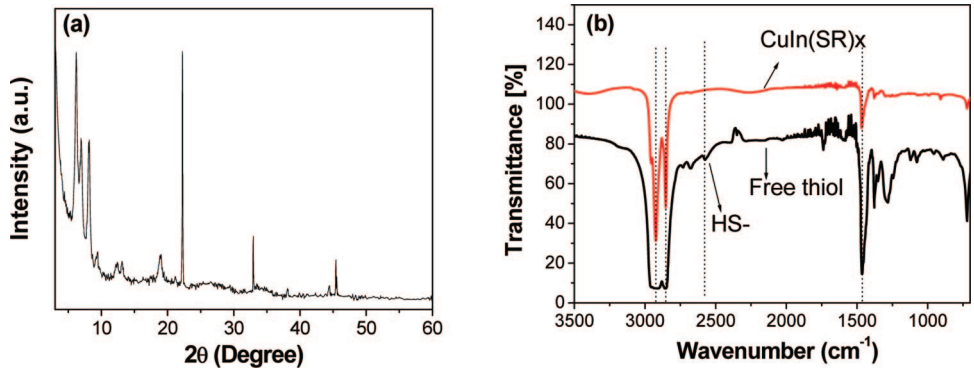

Figure 2. (a) Powder X-ray diffraction pattern of the intermediate compound prepared by the reaction of 0.2 mmol of CuAc, 0.2 mmol of $In(Ac)_3$, and 0.5 mL of dodecanethiol in 5 mL of ODE at 210 °C for 10 min. (b) FTIR spectra of intermediate compound prepared by the reaction of 0.2 mmol of CuAc, 0.2 mmol of $In(Ac)_3$, and 0.5 mL of dodecanethiol in 5 mL of ODE at 210 °C for 10 min and that of pure dodecanethiol.

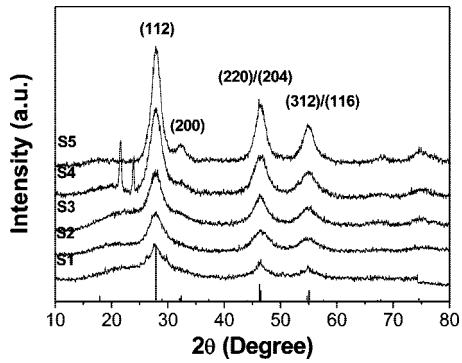

Figure 3. Powder X-ray diffraction patterns of the samples prepared by thermolysis of 0.2 mmol of CuAc, 0.2 mmol of $InAc_3$, and 0.5 mL of dodecanethiol in 5 mL of ODE at 240 °C: sample 1, for 60 min; sample 2, for 120 min; sample 3, for 180 min; sample 4, for 240 min; sample 5, for 180 min with 1 mL of oleic acid added into the reaction system at 120 min.

have the band at 2577 cm^{-1} belonging to S−H vibrations. So, the intermediate compound formed by the reaction of metal salts with dodecanethiol could be $CuIn(SR)_x$. The $CuIn(SR)_x$ complex was further studied by the NMR technique. In the ^1H NMR spectrum of the $CuIn(SR)_x$ complex (see Figure S1 in the Supporting Information), there is a peak at δ 2.60 ppm which is attributed to the hydrogen at SCH_2. This peak is broadened due to the bonding of the sulfur atom to Cu or In metal atoms. In addition, the morphology of the $CuIn(SR)_x$ complex was also studied by TEM observation (see Figure S2a in the Supporting Information). The $CuIn(SR)_x$ complex shows the shape of nanowires with diameter of tens of nanometers and length of several micrometers.

XRD patterns of the samples prepared at 240 °C with reaction time longer than 60 min, as shown in Figure 3, match well with the published tetragonal $CuInS_2$.[25] So it is clear that an intermediate compound of $CuIn(SR)_x$ was first formed and then decomposed into $CuInS_2$ nanoparticles. The sizes of the as-prepared $CuInS_2$ nanoparticles were estimated by the Scherrer formula, and the results are shown in Table 1. It can be seen from Table 1 that the size of the as-prepared $CuInS_2$ nanoparticles increased with the increase of the temperature and reaction time.

Table 1. Average Diameter (D) of the $CuInS_2$ Nanoparticles Determined from the Width of the XRD Peaks According to the Scherrer Formula (Ref 26), TEM Images, and Optical Properties (see Figure S3 in the Supporting Information)

	reaction temperature (°C)	reaction time (h)	D_{XRD} (nm)	D_{TEM} (nm)	$D_{absorption}$ (nm)
sample 1	240	1	1.9	−	2.6
sample 2	240	2	2.2	2.6	2.8
sample 3	240	3	2.6	3.0	3.1
sample 4	240	4	3.1	3.3	3.4
sample 5	240	3[a]	4.3	4.7	4.2

[a] With 1 mL of oleic acid added into the reaction system at 120 min.

Except for XRD characterization, the composition and valence states of the $CuInS_2$ nanoparticles were further investigated by XPS and ICP-AES analysis, as shown in Figure 4. The Cu 2p, In 3d, and S 2p core levels were examined, respectively. The binding energies of Cu 2p, In 3d, and S 2p of $CuInS_2$ are consistent with those reported in literature.[27] The binding energies for Cu 2p 3/2 and Cu 2p 1/2 are in agreement with that of Cu^+ reported by Llanos et al.[28] Since the S 2p has doublet peaks of S 2p1/2 and 2p3/2 due to the spin-orbit coupling, the spectrum of the final product was fitted into two peaks with an energy difference of 1.0 eV. The S 2p1/2 peak at 163.0 eV can be assigned to S coordinated to Cu and In in $CuInS_2$. This binding energy is lower than that of free thiol that is supposed to be at 163.5 eV, which may be related to the binding energy between alkylthiol and particle surface.[24] Inductively coupled plasma atomic emission spectroscopy analysis (Cu, In, S) of the samples revealed that the composition of the nanocrystals is $Cu_{1.0}In_{1.08}S_{2.67}$, which is in good agreement with the stoichiometry of $CuInS_2$. The larger S content may be attributed to the capping thiol ligands existing in the surface of the samples.

TEM observations were also employed to study the $CuInS_2$ nanoparticles. Figure 5 shows the TEM images of the nanoparticles synthesized at various reaction conditions. Parts

(25) Abrahams, S. C.; Bernstein, J. L. *J. Chem. Phys.* **1973**, *59*, 5415–5422.

(26) The mean diameters of the as-prepared nanoparticles were determined by the Scherrer formula $d = 0.94\lambda/B \cos(\theta_B)$, where λ is the X-ray wavelength, B is the full width at half-maximum of the diffraction peak, and θ_B is the half-angle of the diffraction peak on the 2θ scale: (112) and (220) diffraction peaks were calculated and are presented in Table 1.

(27) Wagner, C. D.; Riggs, W. M.; Davis, L. E.; Moulder, J. F.; Muilenberg, G. E. *Handbook of X-Ray Photoelectron Spectroscopy*; Perkin-Elmer Corp.: Eden Prairie, MN, 1978.

(28) Llanos, J.; Buljan, A.; Mujica, C.; Ramirez, R. *J. Alloys Compd.* **1996**, *234*, 40–42.

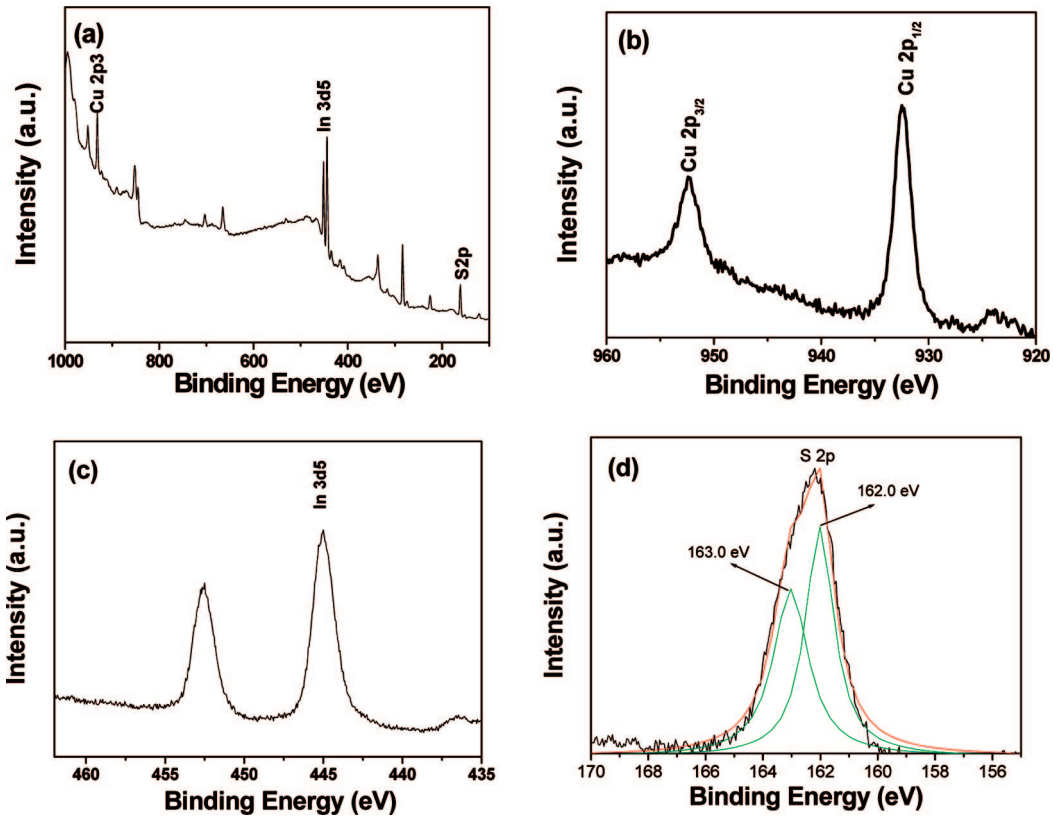

Figure 4. (a) XPS survey spectrum, (b) the XPS spectrum of Cu 2p, (c) the XPS spectrum of In 3d, and (d) the XPS spectrum of S 2p of the $CuInS_2$ nanoparticles prepared by thermolysis of 0.2 mmol of CuAc, 0.2 mmol of $In(Ac)_3$, and 0.5 mL of dodecanethiol in 5 mL of ODE at 240 °C for 180 min.

a−c of Figure 5 show the $CuInS_2$ nanoparticles prepared by thermolysis of the reaction system at 240 °C. After thermolysis for 2 h, the particle size grew into approximately 2.6 nm, which is consistent with the value calculated from XRD data. As the reaction time was prolonged to 3 h, the particle size increased to 3.0 nm and a few elongated rods emerged in the colloidal particles. The HRTEM image of the corresponding nanoparticles is shown in the inset of Figure 5b, where the lattice fringe $d = 0.321$ nm corresponds to the (112) lattice place of tetragonal $CuInS_2$. When the reaction was prolonged to 4 h, elongated rods or multiple rods were formed. The average diameter of the rods is approximately 3.3 nm, and the aspect ratio ranges from 1 to 3. As the reaction time prolonged to 6 h, the formed $CuInS_2$ nanoparticles began to aggregate and precipitate from solution (see Figure 5d). In order to prevent the aggregation of $CuInS_2$, a fixed amount of oleic acid was introduced into the reaction system to stabilize the as-prepared nanoparticles. After adding oleic acid, the elongation of the particles was not observed; only the size of nanoparticles increased with the reaction time prolonged. The TEM image of the as-prepared particles, as presented in Figure 5e, shows that the particles have an average size of 4.7 nm. The size and morphology of the nanoparticles were also influenced by the reaction temperature. When the reaction was performed at 210 °C, it was observed that the color of the solution changed from yellow to red and the absorption spectra shifted from 550 to 630 nm, indicating formation of $CuInS_2$ particles. However, these nanoparticles cannot be directly separated, which may be due to their supersmall size (ca. 1 nm). When the reaction was performed at 270 °C, the precursor decomposed quickly and the as-prepared $CuInS_2$ particles were of large size and broad distribution (see Figure S2b in the Supporting Information). These results indicate that the formation and growth of $CuInS_2$ nanoparticles can be accelerated by the increase of reaction temperature, which is an obvious characteristic of a decomposition reaction.

The HRTEM image shows that most of the particles with rod shapes have a pearl-chain-like structure, which reveals that $CuInS_2$ nanorods may be formed by oriented aggregation. To determine whether the nanorods were formed by an oriented aggregation mechanism, HRTEM images of a series of selected nanoparticles were taken and are shown in Figure 5g−i. It can be seen that the lattice plane of the particles are all aligned along the (112) plane. The lattice planes go straight through the contract areas, and the bottlenecks between the adjacent particles are visible. In some cases, it can be observed that the particles are not aggregated along the axis but have many distortions. The presence of boundaries and defects, which are usually absent in the particles formed by Ostwald ripening, indicates that the nanoparticles were formed by oriented aggregation.[29] The ED pattern of the corresponding particles, as shown in Figure 5i, exhibits a three-ring pattern. These rings correspond to the (112), (220)/(214), (116)/(312) reflection direction of the tetragonal $CuInS_2$.

Formation Mechanism of $CuInS_2$ Nanoparticles. Fundamental understanding of the growth of nanocrystals is of

(29) Penn, R. L. *J. Phys. Chem. B* **2004**, *108*, 12707–12712.

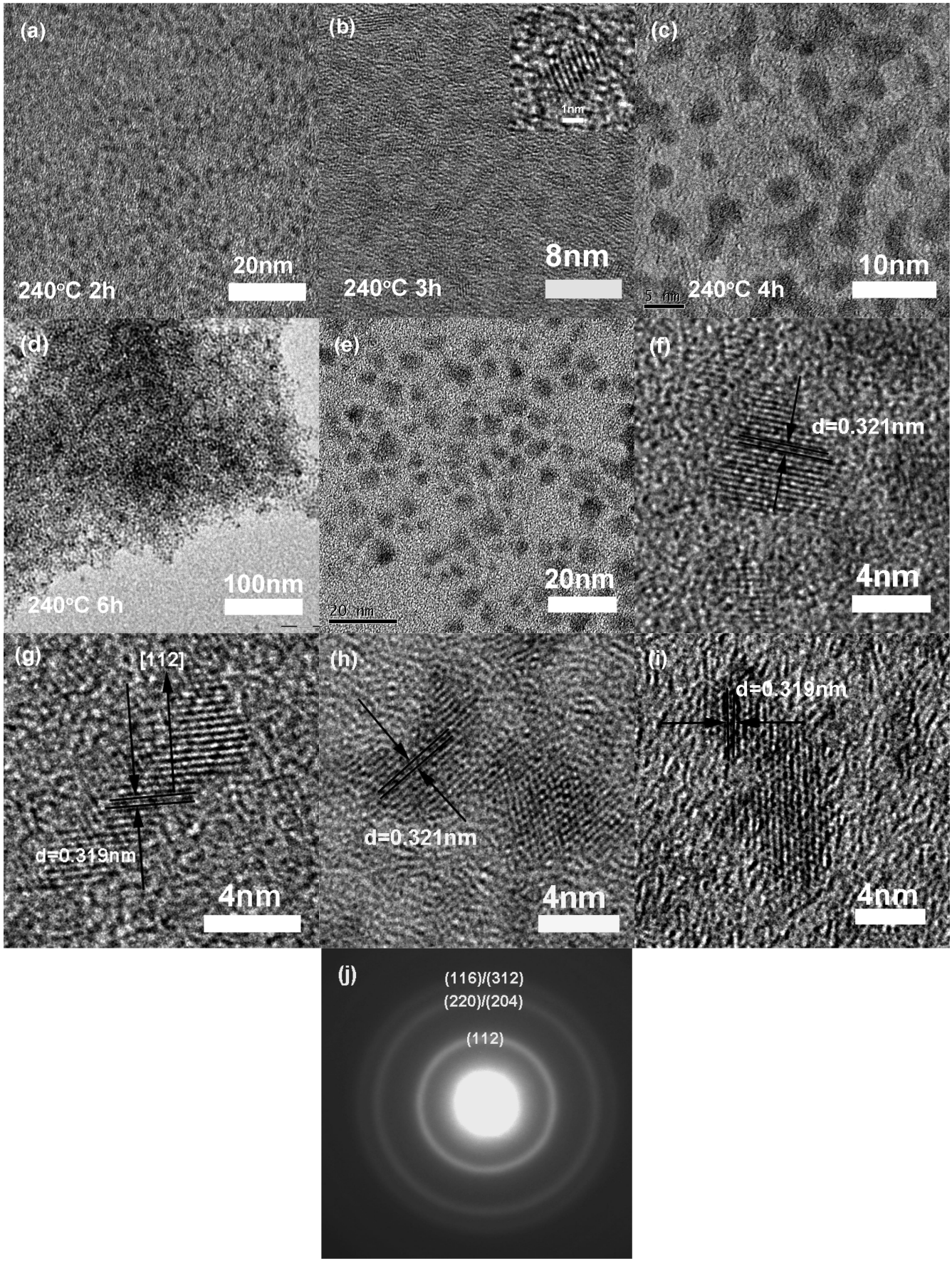

Figure 5. TEM images of the samples prepared by thermolysis of 0.2 mmol of CuAc, 0.2 mmol of $In(Ac)_3$, and 0.5 mL of dodecanethiol in 5 mL of ODE at 240 °C for 120 min (a); for 180 min (sample 3) (b); for 240 min (sample 4) (c); for 360 min (d); for 180 min with 1 mL of oleic acid added into the reaction system at 120 min (sample 5) (e). HRTEM images of sample 5 (f), sample 4 (g−i), and ED pattern (j) of sample 3.

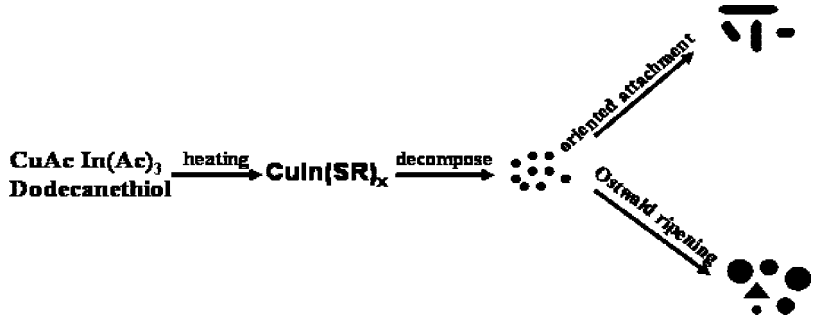

Figure 6. Schematic diagram of the evolution of the morphologies of $CuInS_2$ nanoparticles with reaction temperature and time.

great importance to achieve the designed materials. It was well-known that the growth of nanocrystals in solutions typically involves two processes: fast nucleation and subsequent growth into primary nanoparticles.[29] After the primary particles were formed, the growth of nanoparticles may grow through two primary mechanisms: Ostwald ripening and aggregation. Ostwald ripening occurs through dissolving the monomers from relatively smaller nanocrystals into solution and growing them back onto larger ones among the distribution. Recent works have shown that Ostwald ripening does not adequately describe the growth of some systems where the primary particles were likely to aggregate into secondary particles through mutual attachments. In some cases, the formed secondary particles exhibit preferred structures such as wires, rods, flowers, or uniform spheres.[30] On the basis of these mechanisms, we explained the size and shape evolution of the $CuInS_2$ nanoparticles as follows (see Figure 6). CuAc, $In(Ac)_3$, and dodecanethiol initially reacted to form an intermediate compound of $CuIn(SC_{12}H_{25})_x$ upon heating; then this compound acted as precursor and decomposed into $CuInS_2$ particles, as the reaction time prolonged. After all the precursors were consumed, the growth of $CuInS_2$ nanocrystals could only occur through Ostwald ripening or oriented aggregation. Without oleic acid addition, the as-formed smaller particles are difficult to dissolve and grow into the larger ones; oriented aggregation would be preferred. The $CuInS_2$ particles grow into rods or multiple rods through oriented attaching. With oleic acid addition into the reaction system, the $CuInS_2$ nanocrystals will grow by Ostwald ripening, into large particles with sphere or triangle shapes.

Optical Properties of Colloidal $CuInS_2$ Nanocrystals. Optical properties of colloidal nanocrystals are of great importance for their potential applications as optoelectronic materials.[1] Recently, the size- and shape-dependent optical properties have attracted great attention,[31] while there are few works reported about the optical properties of ternary chalcogenide nanocrystals. For ternary semiconductor nanocrystals, the optical properties can be influenced by at least three factors such as size and shape, surface states, and composition, etc. Figure 7 shows the typical UV−vis absorption spectra, PL spectra, and photoluminescent exciton spectra of the $CuInS_2$ nanoparticles. The absorption spectra of $CuInS_2$ nanoparticles, typically showing a broad shoulder with a trail in the long-wavelength direction, can be tuned to cover the whole visible region. Although there is no obvious absorption peak, the $CuInS_2$ nanoparticles have an absorption edge at around 690 nm, which is significantly blue-shifted from that of bulk $CuInS_2$ (810 nm) and is consistent with the expected quantum confinement effect. The photoluminescence of the nanocrystals is intricate, because it is sensitive to surface structure, crystal sizes and shapes, chemical environment, and a number of interactions.[32] The PL spectrum shown in Figure 7 exhibits a typical emission peak at around 727 nm with a full width at half-maximum (fwhm) of ca. 105 nm. In order to investigate the nature of the broad absorption feature extending into the near-infrared region, which is also present in the PL spectrum of the "as-grown" nanocrystals, we investigated the PLE spectra at several different wavelengths across the PL spectrum. The peak present in the PL spectrum is about 246 meV red-shifted in comparison with the lowest energy feature in the PLE

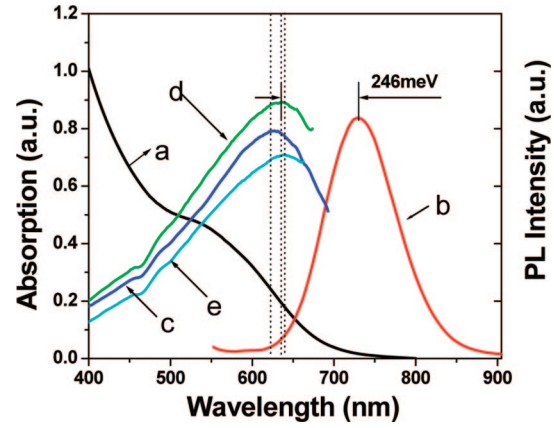

Figure 7. (a) UV−vis absorption, (b) PL (excitation at 540 nm), and (c−e) excitation spectra (emission at 690, 730, and 780 nm, respectively) of a typical $CuInS_2$ nanocrystal solution which was taken from the reaction solution of 0.2 mmol of CuAc, 0.2 mmol of $In(Ac)_3$, and 0.5 mL of dodecanethiol in 5 mL of ODE after thermolysis at 240 °C for 180 min.

(30) (a) Tang, Z. Y.; Kotov, N. A.; Giersig, M. *Science* **2002**, *297*, 237–240. (b) Pacholski, C.; Kornowski, A.; Weller, H. *Angew. Chem., Int. Ed.* **2002**, *41*, 1188–1191. (c) Narayanaswamy, A.; Xu, H. F.; Pradhan, N.; Kim, M.; Peng, X. G. *J. Am. Chem. Soc.* **2006**, *128*, 10310–10319. (d) Zhong, H. Z.; Wei, Z. X.; Ye, M. F.; Yan, Y.; Zhou, Y.; Ding, Y. Q.; Yang, C. H.; Li, Y. F. *Langmuir* **2007**, *23*, 9008–9013.

(31) (a) Alivisatos, A. P. *J. Phys. Chem. B* **1996**, *100*, 13226–13239. (b) Buhro, W. E.; Colvin, V. L. *Nat. Mater.* **2003**, *2*, 138–139. (c) Yu, H.; Li, J. B.; Loomis, R. A.; Wang, L. W.; Buhro, W. E. *Nat. Mater.* **2003**, *2*, 517–520. (d) Zhong, H. Z.; Ye, M. F.; Zhou, Y.; Yang, C. H.; Li, Y. F. *J. Nanosci. Nanotechnol.* **2007**, *7*, 4346–4352.

(32) (a) Weller, H. *Angew. Chem., Int. Ed. Engl.* **1993**, *32*, 41–53. (b) Steigerwald, M. L.; Brus, L. E. *Acc. Chem. Res.* **1990**, *23*, 183–188. (c) Cizeron, J.; Pileni, M. P. *J. Phys. Chem. B* **1997**, *101*, 8887–8901. (d) Nand, J.; Sapra, S.; Sarma, D. D.; Chandrasekharan, N.; Hodes, G. *Chem. Mater.* **2000**, *12*, 1018–1024.

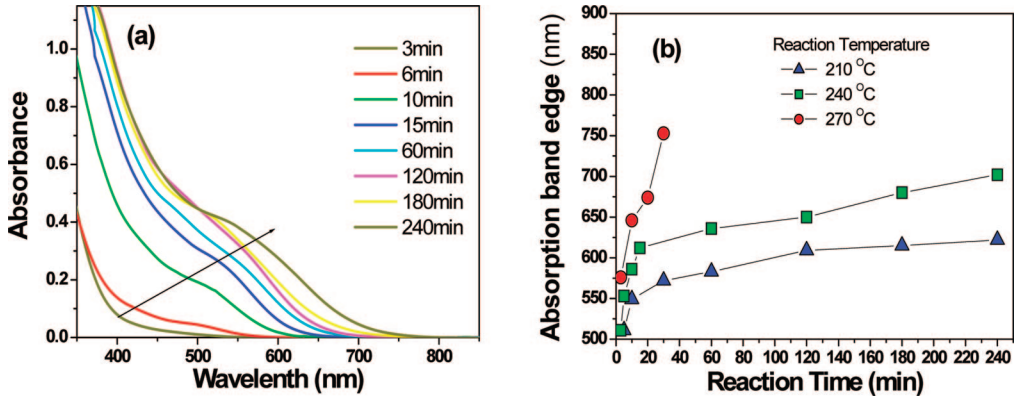

Figure 8. (a) Absorption spectra of the aliquots taken from the reaction solution of 0.2 mmol of CuAc, 0.2 mmol of $In(Ac)_3$, and 0.5 mL of dodecanethiol in 5 mL of ODE after thermolysis at 240 °C for (from left to right) 3, 6, 10, 15, 60, 120, 180, and 240 min. (b) Evolution of absorption edges along with the reaction time for the reaction solution of 0.2 mmol of CuAc, 0.2 mmol of $In(Ac)_3$, and 0.5 mL of dodecanethiol in 5 mL of ODE at 210, 240, and 270 °C, respectively.

spectrum. The peaks of the PLE spectrum fall at the broad tail region, which are at the lower energies than the peak of the absorption spectra. PLE spectra of different emission positions were recorded. It was observed that the peak of the PLE spectrum shift from 621 to 638 nm as the detection wavelength is varied in the range of 660−750 nm. Similar observation was reported by Castro et al.[12b] For the ternary $CuInS_2$ semiconductor, it has been found that a large number of defects (such as donor−acceptor) accompanied with its formation for the composition deviation.[33] The long trailed absorption, broadened emission peaks (fwhm of the peaks is ca. 100 nm), larger stoke shift, and exciton peaks variation are all the characteristics of the optical properties related to the donor−acceptor defects.[12b]

For colloidal semiconductor nanocrystals, the optical properties of these materials have been found to be directly dependent on the size of the nanocrystals. As discussed above, the size of the $CuInS_2$ nanoparticles can be controlled by the reaction time and temperature. It was found that the optical properties of $CuInS_2$ semiconductor nanoparticles can also be tuned by adjusting the reaction temperature and time. Figure 8a shows the evolution of UV−vis absorption spectra of the aliquots, which were taken from the reaction solutions of 0.2 mmol of CuAc, 0.2 mmol of $In(Ac)_3$, 0.5 mL of dodecanethiol in 5 mL of ODE at 240 °C for different times. The absorption wavelength of the $CuInS_2$ nanocrystals increases continuously as a function of growth time until the reaction precursor is exhausted. Obviously, the size of the nanoparticles grows with reaction time and the band gaps decrease with the increase of the nanoparticle size. As reported in literature, the diameters of the nanoparticles can be calculated from the absorption edges by using an effective approximation method.[34] The diameters were calculated as follows:

$$\Delta E_g = (\hbar\pi)^2/2\mu R^2 - 1.786e^2/\varepsilon R; \quad \mu = 1/(1/m_e^* + 1/m_h^*) \tag{1}$$

where ΔE_g is the shift of band gap of the nanoparticle with respect to the bulk semiconductor, R is the particle size, ε is the dielectric constant of the bulk material, m_e^* is the effective electron mass, and m_h^* is the effective hole mass. The values of $CuInS_2$ are 11 for ε_{dot}, 0.16 for m_e^* and 1.3 for m_h^*, respectively. On the basis of eq 1, the relation between the diameter of nanoparticles and absorption edge was plotted (see Figure S3 in the Supporting Information). The diameter of the particles can be directly read out from the curve. Filled circles represent the size of $CuInS_2$ nanoparticles determined by TEM and their band gaps. The experimental data points are compared with the values obtained from the theory. The average diameters of the $CuInS_2$ nanoparticles calculated from the absorption edges are in good agreement with that of TEM observation and that calculated from XRD results. This indicates that the optical properties of $CuInS_2$ nanoparticles exhibit size-dependent properties. The temporal growth dynamic also influenced the shift of absorption edge with the reaction time. Figure 8b shows the temporal evolution of absorption edges along with the reaction time. (The detailed spectra can be found in Figures S4 and S5 in the Supporting Information.) It can be concluded that the size of the particles gradually increased as the reaction time prolonged and the growth of $CuInS_2$ particles was obviously accelerated by increasing the reaction temperature.

Except for the absorption spectra, the PL spectra of $CuInS_2$ nanocrystals also exhibit size-dependent emissions. Figure 9a shows evolution of PL emission spectra of $CuInS_2$ nanoparticles, which also exhibit size-dependent emissions ranging from 630 to 740 nm. When the reaction was performed at 240 °C, the initial reaction solution was not luminescent. With reaction time prolonged to 10 min, the PL emission emerged and the PL peaks gradually shifted from 630 to 740 nm. Unlike the II−VI CdSe synthesis, the fwhm values of the PL emissions are all ca. 105 nm without narrowing. The evolution of PL quantum yields of the solutions was also recorded and is shown in the inset of Figure 9a. It was noted that the PL quantum yield increased up to 5% after reaction for 2 h and then dropped with the size growth.

Surface defects have been attributed to be one of the important factors that may influence the PL intensity. A

(33) Tell, B.; Shay, J. L. *Phys. Lett.* **1971**, *4*, 2463–2469.

(34) (a) Brus, L. E. *J. Phys. Chem.* **1986**, *90*, 2555. (b) Wang, Y.; Suna, A.; Mahler, W.; Kasowski, R. *J. Chem. Phys.* **1987**, *87*, 7315–7322. (c) Wang, Y.; Herron, N. *J. Phys. Chem. B* **1991**, *95*, 525–532.

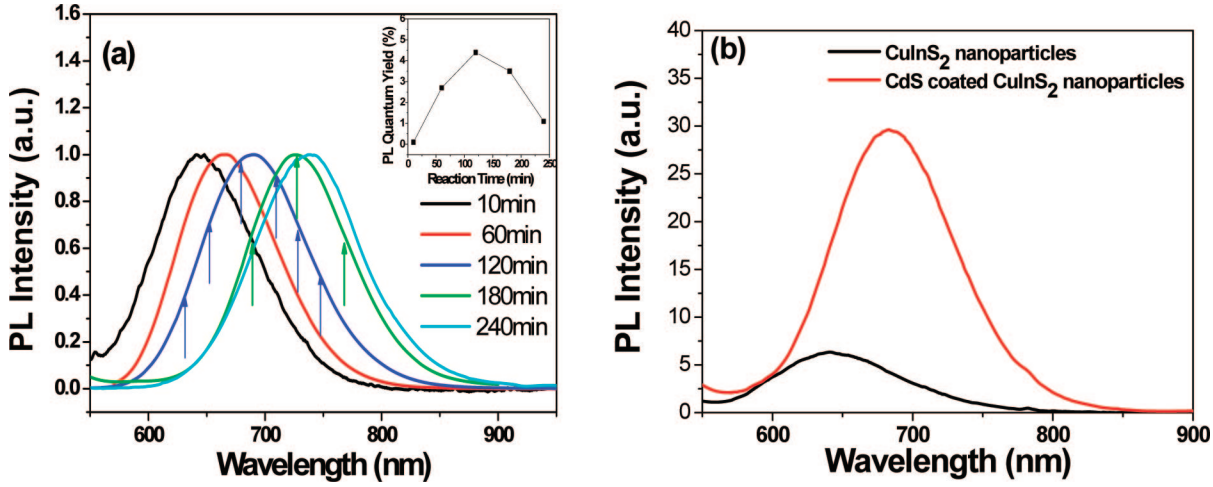

Figure 9. (a) PL spectra of the aliquots taken form the reaction solution of 0.2 mmol of CuAc, 0.2 mmol of $In(Ac)_3$, and 0.5 mL of dodecanethiol in 5 mL of ODE at 240 °C for (from left to right) 10, 60, 120, 180, and 240 min. (b) PL spectra of $CuInS_2$ nanoparticles before and after CdS coating.

proven strategy for reducing the surface defects is to grow a shell of higher band gap semiconductor onto the core nanocrystals.[35] To determine the effects of surface defects on the PL emission, the shell-coating strategy was applied to improve the PL emission quantum yields. The PL emission peak shifted from 640 to 680 nm, and the PL intensity was 5 times increased without any narrowing, by coating CdS layers on the as-prepared $CuInS_2$ nanoparticles (see Figure 9b). This implies that the effect of surface defects has an influence on the PL emission.

It has been discussed that the intrinsic defects, size-dependent band gap, and surface defects are all involved in the PL emission. The radiative lifetime of PL emission is another important optical property of semiconductor nanocrystals that deserves concern.[36] Different radiative lifetimes may correspond to different electron−hole recombination mechanisms. Time-resolved laser techniques are most suitable for probing the lifetime of PL emission. Figure 10 shows the representative PL decay curves of the $CuInS_2$ nanoparticles, which were probed at different emission wavelengths. The PL decay curve for each emission wavelength can be well fitted by a triexponential function:

$$I(t) = A_1 \exp(-t/\tau_1) + A_2 \exp(-t/\tau_2) + A_3 \exp(-t/\tau_3)$$

where τ_1 (τ_2, τ_3) represents the decay time of the PL emission; A_1 (A_2, A_3) represents the amplitude of the decay components at $t = 0$. The constants obtained by the fitting are shown in Table 2, with τ_1 ranging from 4 to 12 ns, τ_2 ranging from 28 to 60 ns, and τ_3 ranging from 140 to 300 ns. It was found that the PL decays of the $CuInS_2$ nanocrystals are wavelength-dependent, with the mean PL decay times increasing with the increase of the PL wavelength. In all the wavelengths of the $CuInS_2$ sample, the amplitude A_3 with radiative lifetime of 140−300 ns accounts for a large amount (40−80%) of the total PL emission spectra. Previous PL decay investigations of CdSe quantum dots have revealed that the radiative time of CdSe colloidal particles has a universal biexponential time distribution.[35] Typically, a shorter lifetime is on the time scale of several nanoseconds, and a longer lifetime is tens of nanoseconds. The shorter lifetime can be attributed to the intrinsic recombination of initially populated core states, and the longer lifetime can be attributed to surface states. For the $CuInS_2$ nanoparticles, the two radiative lifetime

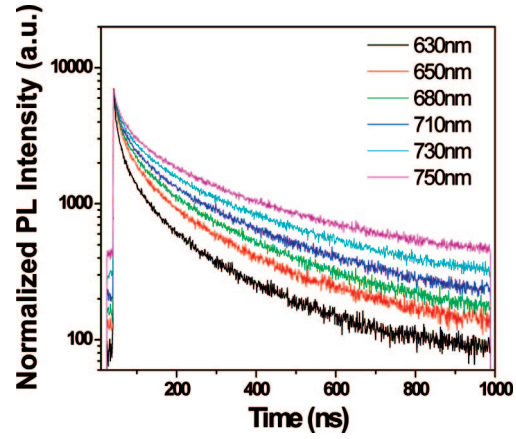

Figure 10. PL decay curves of sample (prepared by heating 0.2 mmol of CuAc, 0.2 mmol of $In(Ac)_3$, and 0.5 mL of dodecanethiol in 5 mL of ODE at 240 °C for 120 min) detected at 630, 650, 680, 710, 730, and 750 nm, respectively.

Table 2. Decay Times and Amplitude Constant Ratios of the PL Emission at Different Wavelengths for Samples 2 and 3 (Prepared by Thermolysis of 0.2 mmol of CuAc, 0.2 mmol of $InAc_3$, and 0.5 mL of Dodecanethiol in 5 mL of ODE at 240 °C for 120 min (Sample 2) or 180 min (Sample 3))

sample	wavelength/nm	τ_1/ns	A_1/%	τ_2/ns	A_2/%	τ_3/ns	A_3/%
sample 2	630	6.3	8.8	41.5	26.6	200.4	64.6
	650	8.3	6.4	46.2	24.5	220.8	69.1
	680	8.6	5.3	50.4	21.5	241.3	73.2
	710	10.2	4.6	57.4	20.6	272.2	74.8
	730	10.8	3.9	60.9	18.6	290.0	77.5
	750	11.3	3.2	57.9	15.5	287.5	81.6
sample 3	690	4.6	17.3	28.0	40.3	143.6	42.4
	730	7.7	10.3	40.9	36.1	186.5	53.6
	770	10.6	7.4	52.6	29.0	221.3	63.6

(35) (a) Li, J. J.; Wang, Y. A.; Guo, W. Z.; Keay, J. C.; Mishima, T. D.; Hohnson, M. B.; Peng, X. G. *J. Am. Chem. Soc.* **2003**, *125*, 12567–12575. (b) Cumberland, S. L.; Hanif, K. M.; Javier, A.; Khitrov, G. A.; Wowssner, S. M.; Yun, C. S. *Chem. Mater.* **2002**, *14*, 1576–1584.

(36) (a) Zhang, J. Z. *Acc. Chem. Res.* **1997**, *30*, 423–429. (b) Kapitonov, A. M.; Stupak, A. P.; Gaponenko, S. V.; Petrov, E. P.; Rogach, A. L.; Eychmuller, A. *J. Phys. Chem. B* **1999**, *103*, 10109–10113. (c) Wang, X. Y.; Qu, L. H.; Zhang, J. Y.; Peng, X. G.; Xiao, M. *Nano Lett.* **2003**, *3*, 1103–1106. (d) Lee, W. Z.; Shu, G. W.; Wang, J. S.; Shen, J. L.; Lin, C. A.; Chang, W. H.; Ruaan, R. C.; Chou, W. C.; Lu, C. H.; Lee, Y. C. *Nanotechnology* **2005**, *16*, 1517–1521.

τ_1 and τ_2 may be assigned to intrinsic recombination of initially populated core states, and surface states, respectively. The long luminescence lifetime (140 to ~300 ns) was attributed to donor−acceptor transition, which can also be deduced from the broad emission peaks (fwhm of the peaks is all ca. 100 nm), low quantum efficiency, and exciton peaks variation. In this sense, the time-resolved measurements indicate that there exist three types of PL radiative mechanisms in the PL spectrum of the as-prepared $CuInS_2$ nanoparticles and the PL emission mainly originates from the intrinsic donor−acceptor transition.

Conclusions

$CuInS_2$ nanoparticles with size of 2 to ~5 nm and nanorods with aspect ratio of 1 to ~3 were controllably synthesized by a simple thermolysis of CuAc, $In(Ac)_3$ and dodecanethiol precursors in a noncoordinating solvent ODE with adjusting of the reaction parameters. Moreover, gram-scale synthesis of ca. 2.0 g of $CuInS_2$ nanocrystals was realized by using the thermolysis method at one time. Powder XRD, TEM, HRTEM, ED, and XPS characterizations showed that the as-prepared $CuInS_2$ nanocrystals are in a tetragonal crystalline structure. A possible growth mechanism to explain the size and shape control of the $CuInS_2$ nanoparticles was proposed and discussed. The absorption and PL emission spectra of the as-prepared $CuInS_2$ nanoparticles were tunable within 550−760 and 600−750 nm, respectively, depending on the size of the nanocrystals and showing size-dependent quantum confined effects. The radiative lifetime of PL emission of the nanocrystals was investigated by the time-resolved PL decay technique. The PL decay curve of the $CuInS_2$ nanoparticles has a triple exponential characteristic with lifetimes of 4−12, 28−60, and 140−300 ns, respectively. The longest lifetime (140−300 ns) occupies a larger amount in the PL emission of the samples. The results imply that the room-temperature PL emission of $CuInS_2$ nanoparticles involves three types of recombination: band exciton recombination, surface-related recombination, and donor−acceptor defects recombination. The PL emission of $CuInS_2$ nanoparticles mainly originates from the donor−acceptor defects.

Acknowledgment. This work was supported by NSFC (Nos. 20721061 and 50633050). The authors thank Dr. Jiang Tang, Professor Fenglian Bai, and Dr. Hailin Qiu for valuable discussions on the synthetic process and optical properties and Ms. Jinhua Cui for the ICP-AES measurements.

Supporting Information Available: Additional NMR spectrum, TEM images, absorption and PL spectra of the $CuInS_2$ nanoparticles, and theoretical band gaps of $CuInS_2$ nanoparticles (PDF). This material is available free of charge via the Internet at http://pubs.acs.org.

CM8006827